A QUANTITATIVE BIFURCATION ANALYSIS OF HÉNON–LIKE 2D MAPS

C. POLYMILIS[1], G. SERVIZI[2] and CH. SKOKOS[1]
[1]*Department of Physics, Athens University, Panepistimiopolis, 15784 Zografos Athens, Greece*
[2]*Department of Mathematics, Bologna University, Italy and I.N.F.N. Sezione di Bologna*

(Received: 17 July 1996; accepted: 8 November 1996)

Abstract. We numerically study the bifurcations of two nonlinear maps, with the same linear part, which depend on a parameter namely the Hénon quadratic map and the so called 'beam-beam' map. Many families of periodic orbits which bifurcate from the central family, are studied. Each family undergoes a sequence of period doubling bifurcations in the quadratic map. But the behavior of the 'beam-beam' map is completely different. Inverse bifurcations occur in both maps. But some families of the same type which bifurcate inversely in the quadratic map do not bifurcate inversely in the 'beam-beam' map, even though both maps have common linear part.

Key words: bifurcations, maps

1. Introduction

A basic model with applications in many branches of physics is the Hénon quadratic map [1, 2, 3]. The Poincaré sections of any 2 degrees of freedom hamiltonian system is a generic area preserving map of which the Hénon map captures the main relevant features.

The Hénon conservative quadratic map is of the form [1]

$$\begin{aligned} x' &= 1 - y \pm ax^2 \\ y' &= x. \end{aligned} \tag{1}$$

When the parameter a ranges in the interval $(-3, 1)$ and $a \neq 0$, the map (1), with the sign (+) in front of the nonlinear term, can be transformed to a map of the form

$$\begin{pmatrix} x \\ y \end{pmatrix}' = \mathbf{R}(\omega) \begin{pmatrix} x \\ y + x^2 \end{pmatrix} \tag{2}$$

by identifying $\cos(2\pi\omega)$ with the value $1 - \sqrt{1-a}$.

In (2) we consider $\mathbf{R}(\omega)$ to be the orthogonal matrix

$$\mathbf{R}(\omega) = \begin{pmatrix} \cos(2\pi\omega) & \sin(2\pi\omega) \\ -\sin(2\pi\omega) & \cos(2\pi\omega) \end{pmatrix}.$$

The parameters a and ω are related through

$$a = 1 - 4\sin^4(\pi\omega), \quad -3 < a < 1, \quad a \neq 0. \tag{3}$$

Celestial Mechanics and Dynamical Astronomy **66:** 365–385, 1997.

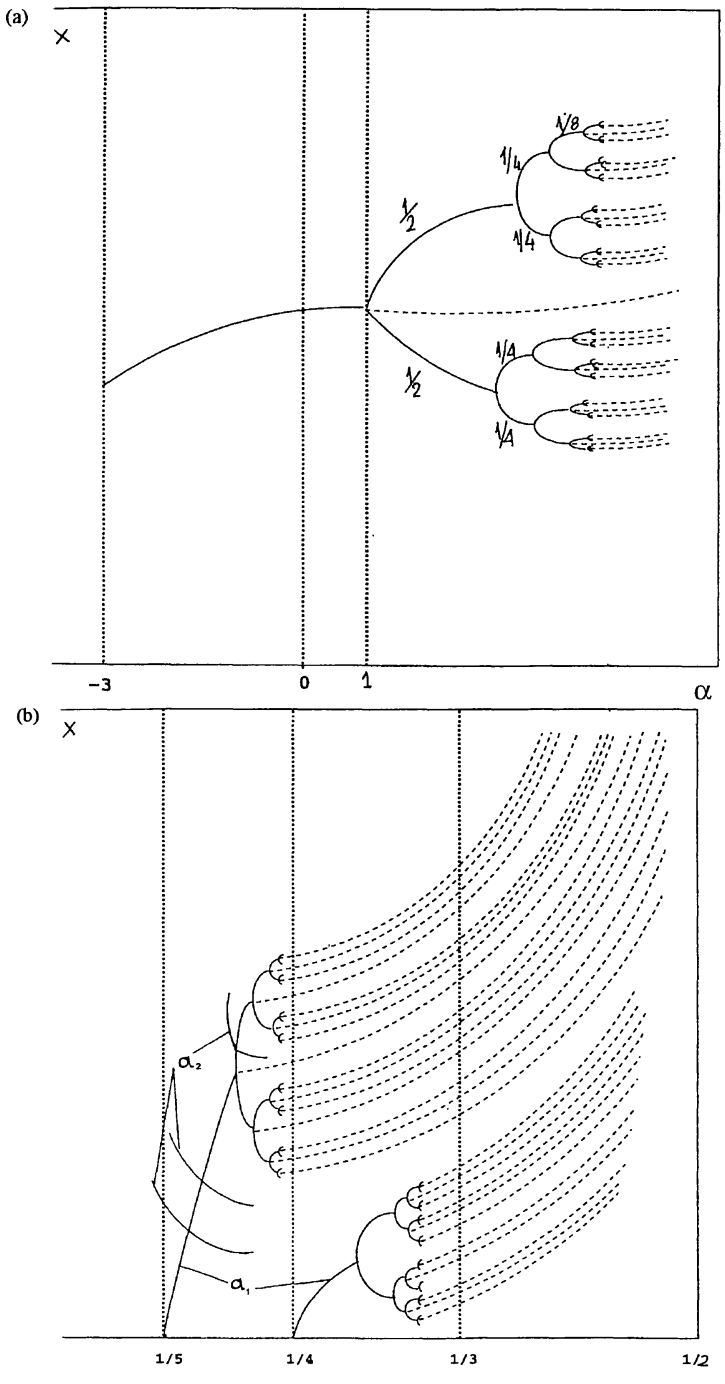

Figure 1. The characteristic curves of the central families of the quadratic map (1) (with sign (+)) and of the transformed map (2), schematically: (a) For the values of the parameter a in the interval $(-3, 1)$ the central family of the quadratic map (1) is stable. For values of $a > 1$ this family becomes unstable and period dubling bifurcations of multiplicity 2^k are born. These bifurcations have been studied by Bountis [4]. (b) The characteristic curve of the central family of the rotational map (2) coincides with the ω-axis ($x = 0$). This characteristic, for values of ω in the interval $(0, \frac{1}{2})$, corresponds to the stable part of the characteristic of the quadratic map (the parameter a ranging in the interval $(-3, 1)$ in the above Figure a). We see also, schematically, some primary a_1 and secondary a_2 resonant families. The unstable bifurcating families tend to infinity, remaining unstable, as $\omega \to \pi$. The phase plane of this map has been studied by Hénon.

On the other hand, taking the $(-)$ sign in front of the nonlinear term of the map (1) we transform it to (2) by putting $\cos(2\pi\omega) = 1 - \sqrt{1+a}$ with a ranging in the interval $(-1, 3)$ and $a \neq 0$. Then the relation between the parameters a and ω reads

$$a = -1 + 4\sin^4(\pi\omega), \quad -1 < a < 3, \quad a \neq 0. \tag{4}$$

The trasformations of the Hénon map (1) to the map (2) is proven in the Appendix (see also [1]). In Figures 1a and 1b we draw schematically the characteristics of the central families of periodic orbits of the quadratic map (1) with the sign $(+)$ and of the map (2) with respect to the parameters a and ω respectively. In the quadratic map (1), for values of a in the interval $(-3, 1)$ the central family is stable (Figure 1a) while for values $a > 1$ it is unstable. In the map (2), the characteristic of the central family coincides with the axis $x = 0$ (Figure 1b) and it is stable for any value of ω. According to the relation (3) or (4), when the parameter ω ranging in the interval $[0, \frac{1}{2}]$ the transformed map (2) represents the quadratic map (1) when the parameter a ranging in the interval $[-3, 1]$ or $[-1, 3]$.

In what follows we call the transformed map (2) as rotational map. Thus the rotational map represents the dynamics of the quadratic map for values of the parameter at which its central family is stable.

Hénon [1] studied the main properties of the rotational map by calculating many trajectories on the phase plane for several values of the parameter and he found the fixed points, both analytically and numerically up to multiplicity 4 and 76 respectively.

For the values of the parameter at which the central family of the qudratic map is unstable a sequence of period doubling bifurcations exists. The first family of this sequence is born from the central family, when its stability character changes. These period doubling bifurcations have been studied by Bountis [4].

He has shown that the ratio of the successive intervals of the parameter values at which the period doubling bifurcations occur, tends to the universal constant, $\delta \simeq 8.7210\ldots$. These bifurcating families consist of fixed points of multiplicity 2^k and the universal ratio is obtained when $k \to \infty$, at a finite value of the parameter of the nonlinearity of the system. We notice that the problem of the bifurcations of periodic orbits in hamiltonian systems with two degrees of freedom has been widely investigated [5, 6] while universal properties in families of periodic orbits of conservative maps has also been found [7, 8, 9].

However, in the quadratic map, except the bifurcating family of multiplicity 2, there exist other families of fixed points, which bifurcate from the stable part of the central family. Thus, in order to understand the dynamics of the quadratic map the study of the bifurcations of the rotational map is necessary.

In this paper, the results of Hénon [1] are completed by investigating in detail the bifurcations of the rotational map and in combination with those of Bountis [4]

the complete dynamics of the quadratic map is obtained. We also define a class of maps which have common linear part with the quadratic one. These Hénon like maps are of considerable interest in many physical applications [3] and we proceed to a first discussion of one of them, the so-called 'beam-beam' map.

The investigation of the properties of the rotational and the 'beam-beam' map, as their linear frequencies vary, is performed by constructing the corresponding diagram of characteristic curves, by combining two powerful numerical tools which allow high periods to be reached: an efficient algorithm for the computation of solutions of both algebraic and transcendental systems of equations [10] and an interactive driver to visualize the phase space of a two dimensional map on a workstation's screen [11].

An infinity of characteristics bifurcate from the central family of both maps, corresponding to an infinity of resonances of different multiplicity. Such resonances correspond to periodic orbits of a hamiltonian system and their theoretical prediction was made by Poincaré [12] ('solutions periodiques du deuxiéme genre'). These resonances correspond to the rationals of a Farey tree.

We study the characteristic curves of the resonances $\frac{1}{n}$ with $3 \leq n \leq 9$. All the resonances of the rotational map, except the resonance $\frac{1}{3}$, behave qualitatively in a similar way. In the case of the 'beam-beam' map the bifurcated families of the same period with those of the rotational map behave in a completely different way.

It is well known that the inverse bifurcations in a dynamical system, if they exist, strongly influence the dynamical behaviour of the system [13, 14]. In the maps in hand, the behavior of the $\frac{1}{3}$ characteristics allow us to conjecture the existence of inverse bifurcations in both maps. We have indeed located some of them numerically, using information from the corresponding Farey trees.

An interesting result is that some inverse bifurcations that exist in the rotational map are not inverse in the 'beam-beam' map despite the fact that both maps possess common linear parts.

In the rotational map the hyperbolic fixed points of any multiplicity go very fast towards infinity as the parameter tends to the end point of its domain of existence, while in the 'beam-beam' map this does not happen because the motion is bounded.

The paper is organized as following. In Section 2 we discuss the character of the maps we deal with and the correspondence between the bifurcating families and the Farey tree sequence. In Section 3 we describe the interactive technique adopted to compute and follow fixed points, as the parameter changes. In Section 4 we study numerically many families of fixed points, as the parameter varies, and we discuss in detail their behavior. In the last Section 5 our main conclusions are presented.

2. Hénon–like maps. Bifurcating families

We define an area preserving map depending on a real parameter ω, as follows:

$$\begin{aligned} x' &= -x\cos(2\pi\omega) + (y + h(x))\sin(2\pi\omega) \\ y' &= -x\sin(2\pi\omega) + (y + h(x))\cos(2\pi\omega) \end{aligned} \tag{5}$$

or, equivalently,

$$\begin{pmatrix} x \\ y \end{pmatrix}' = \mathbf{R}(\omega)\begin{pmatrix} x \\ y + h(x) \end{pmatrix}. \tag{6}$$

In (6) we consider $\mathbf{R}(\omega)$ to be the same matrix as in map (2). Due to the particular form of the map (6), its Jacobian is given by the determinant of $\mathbf{R}(\omega)$ which is equal to one. We also consider that the form of the function $h(x)$ is such that vanishes at $x = 0$ together with its first derivative.

Choosing in (6) different functions $h(x)$ we obtain a variety of maps with the same linear part while changing the form of $\mathbf{R}(\omega)$, keeping the value of the determinant equal to 1, other classes of maps can be found. Among such maps we have the rotational Hénon map (2) if we use in equation (5) $h(x) = x^2$, $\mathbf{R}(-\omega)$ and (x, y) with opposite signs, while for $h(x) = 1 - \exp(-x^2)$ we get the so-called 'beam-beam' map. We limit ourselves, however, to these two maps namely to the rotational map and to the 'beam-beam' map.

We notice that, in any case, the parameter ω lies in the domain $[0, \frac{1}{2}]$ rather than $[0, 1]$ since in the second half of the unit interval $\mathbf{R}(\omega)$ takes the same values as in the first half, differing only by a transposition which does not affect the phase space topology [1]. This implies that the resonant value $\omega = \frac{1}{2}$ is a very particular one, since for $\omega = \frac{1}{2}$, any initial point in the plane belongs to a period two cycle for both the rotational and the 'beam-beam' map, that is in both cases the square of the map is the identity.

The 'motion' in the rotational map is unbounded while in the 'beam-beam' one it is bounded. Thus trajectories starting from initial points far enough from the origin do escape to infinity for the rotational map while they remain at finite distance for the 'beam-beam' one. These different behaviors are shown in the corresponding phase space plots (Figure 2). The outer trajectories in the quadratic map (Figure 2a) after some iterations go to infinity while the trajectories with the same initial conditions in the 'beam-beam' map form invariant curves (Figure 2b). Furthermore in the 'beam-beam' map there exist KAM curves in the neighborhood of infinity and this is due to the vanishing nonlinearity.

At this point we notice that if one is needed to investigate transport mechanisms and the diffusion process in the quadratic map and the 'beam-beam' map the difference, of bounded or unbounded motion, between the maps must be taken into acount. The justification is the following: It is well known that in a dynamical

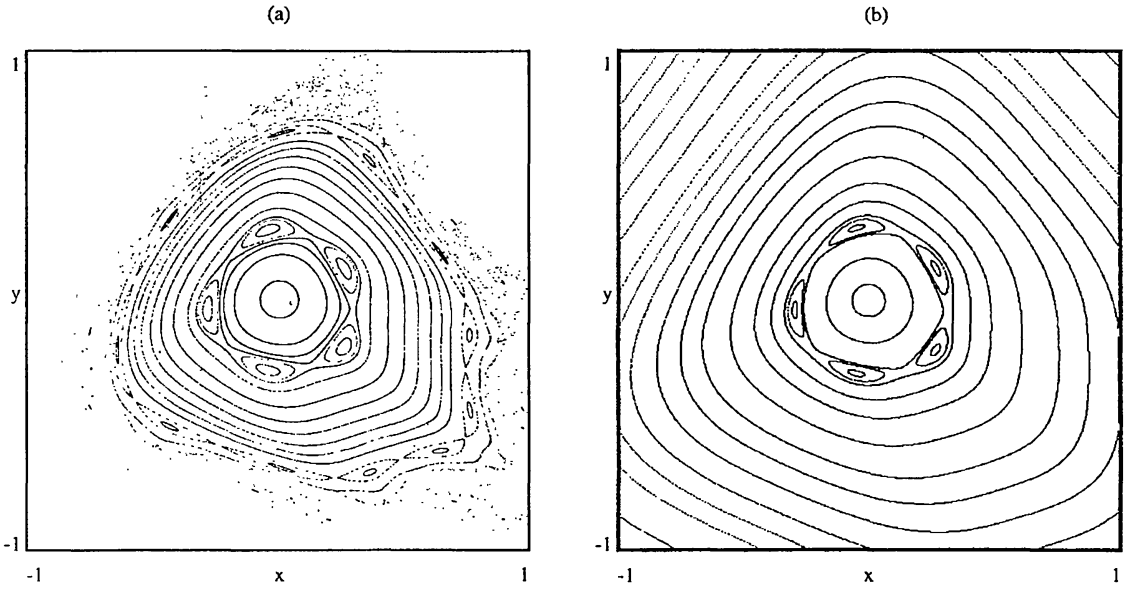

Figure 2. Phase space plots of the rotational map (a) and the 'beam-beam' map (b) for $\omega = 0.203$. The phase space portraits look similar to the neighborhood of the origin, since both maps have the same linear part. Differences can be seen away from the origin. The outer trajectories marked by dots in (a) of the rotatioanal map escape to infinity but they form invariant curves in the 'beam-beam' map (b). The motion in the rotational map is unbounded while in the 'beam-beam' map is bounded.

system the transport phenomena depend on the behavior of the heteroclinic tangles. These tangles are formed by the intersections of the homoclinic ones. However the behavior of the homoclinic tangles is different depending on whether the motion is bounded or unbounded [15].

The Hénon stability index [16] of any fixed point is defined as half the sum of the eigenvalues of the corresponding Jacobian matrix. In other words the Hénon stability index is one half of the trace of the jacobian matrix corresponding to the fixed points of the central family. This index for the fixed points of the central family of both rotational and 'beam-beam' maps, is the same, namely

$$\alpha = \cos(2\pi\omega).$$

It is evident that as the parameter ω varies in the interval $[0, \frac{1}{2}]$ the stability index α decreases continuously and monotonically from $+1$ to -1 which means that the central family is stable. This monotonical behaviour of the stability index α in this interval allows us to associate at each value of α a rational $\frac{m}{n}$ value of ω, where m, n are prime integers with $m < n$ and $n \geq 1$. Thus at any value of ω a new family of fixed points bifurcates, corresponding to the resonance $\frac{m}{n}$ [16]. In other words a fixed point of of the nth composition of the mapping with itself, is born. This type of resonances are of the same type as those occurring in hamiltonian systems and we call them, keeping the same terminology, bifurcations of second genus. They correspond to periodic orbits of which the theoretical prediction was made by Poincaré [12] ('solutions periodiques du deuxième genre', in [12]). All these resonances correspond to the rationals of a Farey tree.

It is well known that a Farey tree is obtained by defining its zeroth generation consisting of a pair of rationals $\frac{m_1}{n_1}$ and $\frac{m_2}{n_2}$ with $m_1n_2 - m_2n_1 = \pm 1$. Such rationals are called 'neighboring'. A rational between two neighbors is obtained by adding numerators and denominators $\frac{m_3}{n_3} = \frac{m_1+m_2}{n_1+n_2}$. This last rational is a neighbor to both rationals of the zeroth generation. By continuing this construction, we obtain every rational in the interval $[\frac{m_1}{n_1}, \frac{m_2}{n_2}]$ which appears once on the tree.

In our case we obtain all the resonances $\frac{m}{n}$ by constructing the Farey tree in the interval $[\frac{0}{1}, \frac{1}{2}]$ which corresponds to the values of ω in the interval $[0, \frac{1}{2}]$.

We emphasize that, the linear part of both maps are the same and since the fixed points of their central families are located at $x = y = 0$ for any value of ω, the Hénon's stability index is the same. This means that at the same value of ω the bifurcating resonances, in both maps, correspond to the same Farey tree.

3. The fixed points calculating procedure

We have performed a systematic numerical study of map (2) using the software package [10] which allows us to interactively draw phase space trajectories of the map and to search for fixed points of any period, starting from an initial guess which can be chosen by direct inspection of the phase portrait visualized on the workstation's monitor. The fixed point computation algorithm has been provided by Vrahatis [11] and is based on the 'characteristic polyhedron' method. It has proven to be a very efficient tool, both fast and accurate, although it works if and only if the initial guess is a box containing the fixed point to be found and no other fixed points of the same period. In the bifurcation problem, two fixed points of the same period arise very close to each other. This implies that a very detailed rendering of the phase portrait trajectories is required and this is not a hard problem since we were able to find e.g. the three hyperbolic fixed points which lie as close as 10^{-10} to the origin for $\omega = 0.3333\ldots$ in the quadratic map.

We start from a value of ω slightly above the resonant value of our interest and draw a phase portrait of the map. Using the fixed points searching algorithm we compute, for instance, the exact position (x, y) of an elliptic fixed point and evaluate the eigenvalues of the mapping $T^{(n)}$ which is tangent in (x, y) to the nth composition of the map (2) with itself. These eigenvalues, or equivalently the stability index [16], give the elliptic or hyperbolic nature of the fixed point. When a family of fixed points first pops up, the map $T^{(n)}$ is tangent to the identity transformation, and its two eigenvalues turn out to be very close to 1. Then the program follows the chosen fixed point when it starts moving in the plane as the parameter ω increases. In order to make the machinery to work correctly, some cautions should be taken: first of all we have to choose the increment of the parameter ω small enough to prevent losing the fixed point after a few steps and secondly we must start with a good estimation of the initial position of the fixed

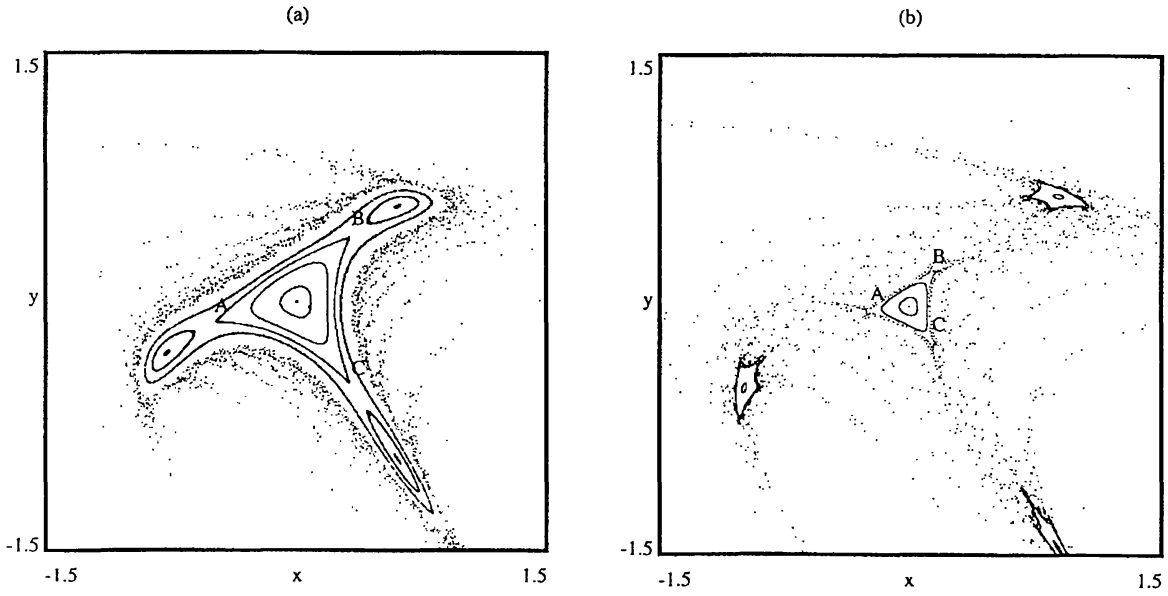

Figure 3. Phase space plots of the rotational map for (a) $\omega = 0.319$ and (b) $\omega = 0.325$ in the same scale. The 3 stable fixed points move away from the central family as ω tends to $\frac{1}{3}$ and the 3 unstable fixed points A,B and C move towards it.

point. We further observe that the closer two neighboring fixed points of the same period are, the smaller would be the value of the increment of ω to find them.

4. Numerical results

To understand in more detail the behavior of the maps we construct many phase portraits of both maps by calculating trajectories for several values of the parameter ω. As already mentioned, when the real parameter ω in (2) passes through a rational value $\frac{m}{n}$, a resonance of multiplicity n is born by bifurcation.

In general, as ω increases from its 'resonant value', the n elliptic and the n hyperbolic fixed points move outwards and n thin islands show up, around the elliptic fixed points. Of course only resonances with small denominator n can be easily seen in the phase portraits. Both maps exhibit cycles of fixed points of the same multiplicity very close to the central fixed point. However the 'beam-beam' map presents also other cycles of fixed points of the same as above period, which come from the region far from the central family. This is due essentially to the fact that the linear part of the transformation in both maps is the same but they differ completely for large $|x|$ because the 'beam-beam' map is bounded while the quadratic one is not.

We emphasize that the phase portraits of both maps look very similar in a small enough neighborhood of the central fixed point. This is due to the fact that the linear parts of both maps are the same since for small $|x|$ we could safely replace $1 - \exp(-x^2)$ by x^2.

A different behavior is observed for the resonance $\frac{1}{3}$ (see also [1]). In the rotational map the three elliptic and three hyperbolic fixed points show up at a finite distance from the central family when $\omega = \omega_{3\,\min} = 0.31797167$ which is smaller than the anticipated value $\omega = \omega_3 = \frac{1}{3} = 0.33333333$. This can be seen in the phase space plot of the quadratic map for $\omega = 0.319$ (Figure 3a). As ω increases remaining below ω_3 the stable fixed points, which are surrounded by islands, move away from the central family, while the hyperbolic ones move towards it (Figure 3b). When ω reaches the value $\omega_3 = \frac{1}{3}$ the three elliptic points become hyperbolic and the hyperbolic points coincide on the central family. Thus, at the value ω_3, no invariant curves exist, around the stable fixed point of the central family. The non existence of invariant curves in the case of the $\frac{1}{3}$ resonance has been proved, in general, by Moser [17], but it has been explicitly proved for the quadratic map by Siegel [18].

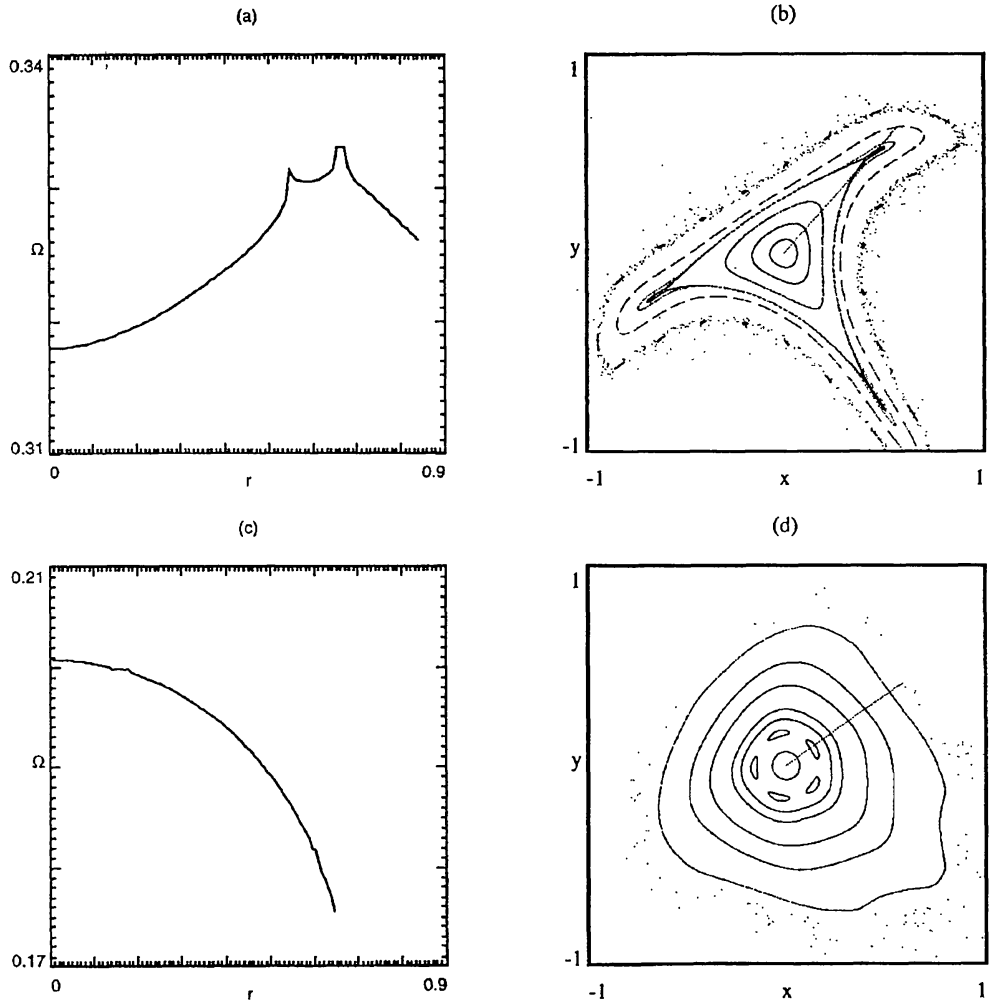

Figure 4. The winding number Ω with respect to the distance r from the origin (a), along a line on the phase space (b) for $\omega = 0.318$, where the resonance $\frac{1}{3}$ is visible. (c) and (d) are similar figures to the previous ones for $\omega = 0.201$ where the resonance $\frac{1}{5}$ exists. All figures are for the rotational map.

The behavior of the resonance $\frac{1}{3}$ can be understood by the behavior of the winding number $\Omega(x^2 + y^2; \omega)$ of the map in normal form [3]. It can be shown that Ω is monotonically decreasing from its value at $x = y = 0$, which is equal to ω, for all ω except a small interval around the value ω_3. This behavior is seen in (Figure 4a) for $\omega = 0.318$, along the line marked in Figure 4b. We see that Ω is equal to 0.318 on the central family and increases as we move away from it. Then in the region where the island of the resonance is located, it changes its behavior and away from this region it decreases. This is due to the fact that 3 fixed points appeared for $\omega = \omega_{3min} < \omega_3$. In Figure 4c we see a plot similar to Figure 4a for $\omega = 0.201$ where the resonance $\frac{1}{5}$ exists (Figure 4d). Thus the different behaviors become evident.

To better understand the dynamics of the systems we construct the diagram of the characteristic curves of several resonances. We draw schematically some of them in Figure 1b. In our case the characteristics are calculated on the plane (ω, y) or (ω, x) where y or x is one coordinate of a fixed point at the corresponding value of ω. The characteristic of the central family of both maps coincide with the ω axis, that is for any ω the corresponding fixed points are located in the origin $x = y = 0$ and we numerically study the characteristic curves of the resonances $\frac{1}{n}$ with $3 \leq n \leq 9$. We discuss the characteristics of the rotational map in detail while in the 'beam-beam' one a first approach is made.

As far as the rotational map is concerned the positions of the fixed points up to the multiplicity 4, are analytically known as functions of the parameter ω [1]. For

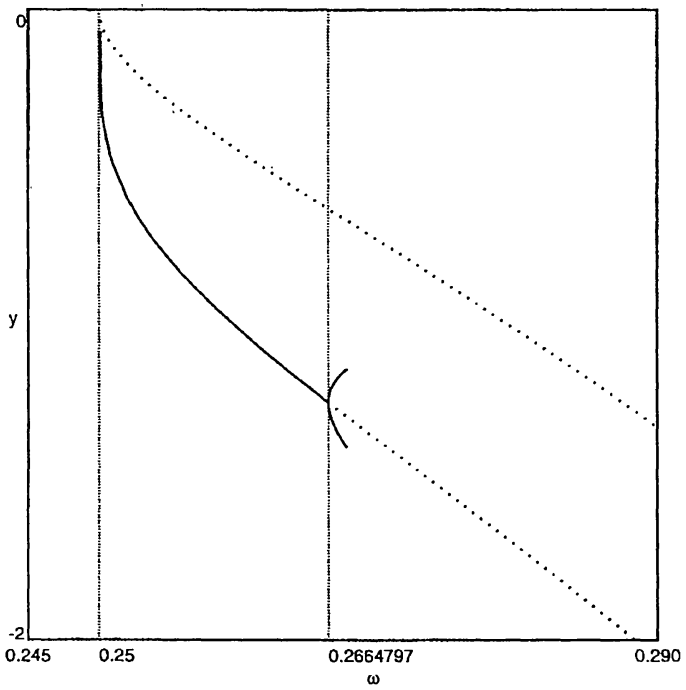

Figure 5. The characteristic diagram of the resonance $\frac{1}{4}$ of the rotational map. The stable (continuous line) and unstable (dotted line) branches of the resonance bifurcate from the central family for $\omega = 0.25$. The stable one undergoes a period doubling bifurcation for $\omega = 0.26648$.

$\omega = \omega_4 = \frac{1}{4}$ two families of fixed points of multiplicity 4 bifurcate from the central one. One of them corresponds to elliptic (stable) and the other one to hyperbolic (unstable) fixed points and the stability index, at ω_4 is $+1$. The characteristic diagram of these families is seen in Figure 5. Their minimum with respect to the parameter ω is on the central family at ω_4. The unstable fixed point (marked by dots in Figure 5) escapes to infinity as ω increases, remaining always unstable. On the other hand the stable fixed point, which is marked by a continuous line, moves away from the central family. At the value $\omega = \omega_{4a} = 0.26648$ the stability index of the corresponding fixed point is -1. Then this stable branch becomes unstable, and as ω increases further the fixed point remains unstable escaping to infinity. At ω_{4a} a family of fixed points of multiplicity 8 bifurcates. This family undergoes a new period doubling bifurcation for a little higher value of ω, and two new families of fixed points of multiplicity 16 are born, and so on. For values of ω greater than $\omega = \omega_{4\delta} = 0.268614$ all the families of this sequence are unstable. For ω smaller than $\omega_{4\delta}$ but close to it we obtain an infinity of period doubling bifurcations. By applying Feigenbaum's definition [19] we obtain the well known 'universal ratio' between successive intervals of bifurcations $\delta = 8.7209$ which has been found for the map (1) by Bountis [4].

A more detailed study is made for the resonance $\frac{1}{5}$ of the rotational map, since no analytical results are available. In this resonance we get a similar behavior as in the $\frac{1}{4}$ one. Two families of fixed points, of multiplicity 5, one stable and the other unstable, bifurcate from the central family for $\omega = \omega_5 = \frac{1}{5}$. Their minimum is also on the central family. The stable branch undergoes a sequence of period doubling bifurcations, as before. We follow these bifurcations up to the family of period 320, which means six successive bifurcations. The computation of the positions of the fixed points of multiplicity 320 was at the limit of our numerical accuracy.

In the following table we see the values of the parameter ω at which the period doubling bifurcations occur. We observe that the differences between these values tend to zero, which means that the values of ω tend to a value $\omega_{5\delta}$ where all the bifurcating branches become unstable. This value is found to be $\omega_{5\delta} = 0.230958867161$.

Table I

from	to	ω
5	10	0.229494194231
10	20	0.230772581264
20	40	0.230937461434
40	80	0.230956408129
80	160	0.230958585186
160	320	0.230958834828

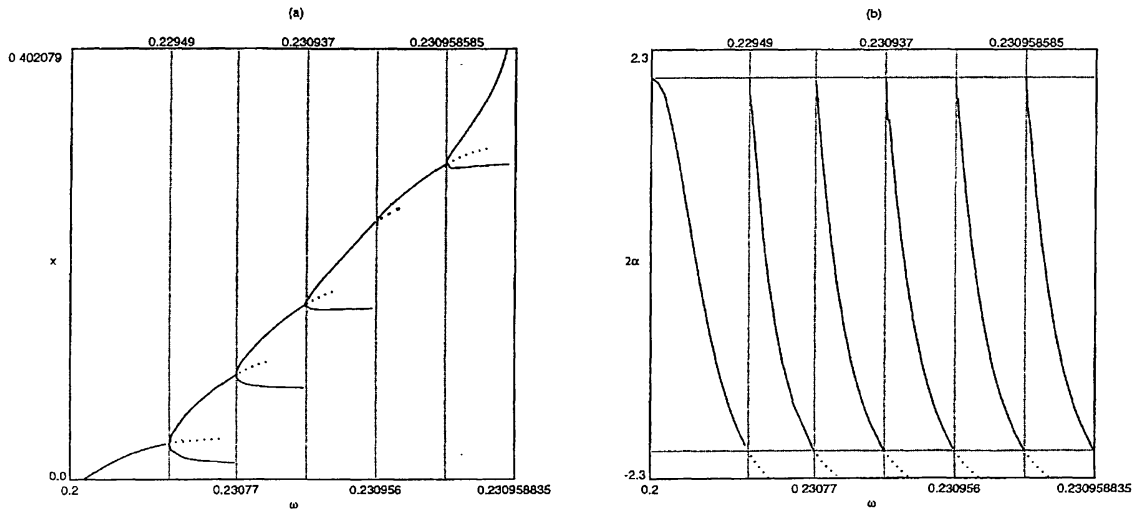

Figure 6. (a) The diagram of the characteristic curves of the family $\frac{1}{5}$ and the resonances bifurcating from it, for the rotational map. We use logarithmic axis so that the bifurcation tree is clearly seen. (b) The stability index 2α of the families of (a).

Using the data of the previous table we get the following one

Table II

n	δ_n
2	7.7534310706
3	8.7023182671
4	8.7028934016
5	8.7207160648

We observe in the above table that as ω reaches $\omega_{5\delta}$ the quantity δ, tends to its universal value.

In Figure 6a we draw the characteristic diagram of these families. As we already saw the values of the parameter where the period doubling bifurcations occur get closer and closer, thus the characteristic curves would not be clear when we have fixed points of high multiplicity. So instead of plotting the characteristic diagram with respect to ω we use $-\log(\omega_{5\delta} - \omega)$ and so all the regions of the bifurcation tree are visible. For the same reason we use $-\log(|x^*| - |x|)$ instead of x, where x^* is near the maximum value of x relative to the current family.

In Figure 6b we plot the trace of the jacobian matrix corresponding to the fixed points of Figure 6a with respect to $-\log(\omega_{5\delta} - \omega)$. The trace is the Hénon's stability index α multiplied by 2. We see that it decreases monotonically from $+2$ to -2 for every bifurcating family. This means that each bifurcated family in the corresponding range of values of ω is stable. Thus, in general, from the stable branch of each bifurcated family secondary resonances are born again by bifurcations. We

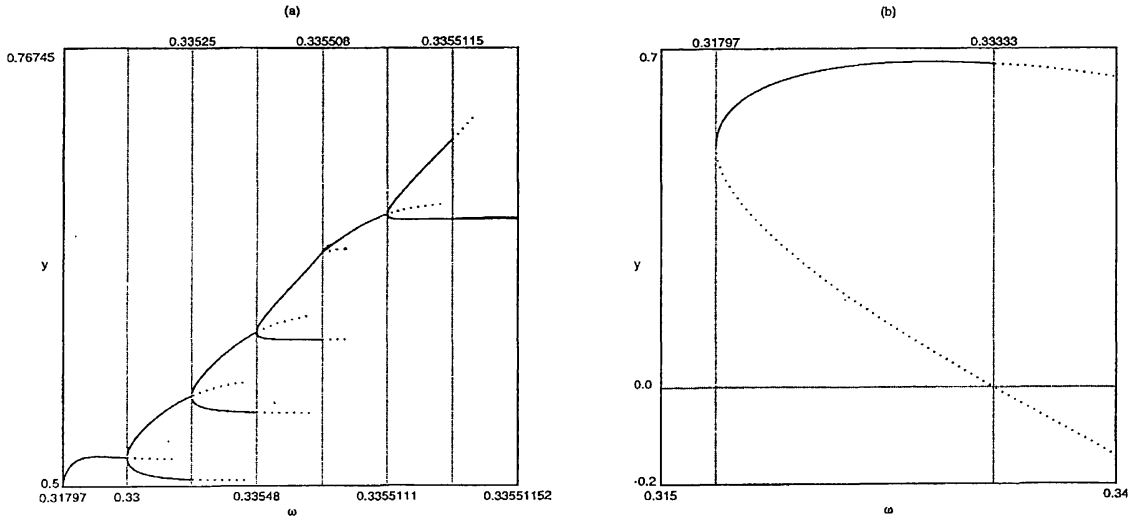

Figure 7. (a) The diagram of the characteristic curves of the family $\frac{1}{3}$ and the resonances bifurcating from it, for the rotational map. We use logarithmic axis as in Figure 3a. (b) An enlargement of figure (a) where we see that resonance $\frac{1}{3}$ is born by bifurcation and the corresponding characteristic curve crosses obliquely the characteristic of the central family.

draw schematically some of them in Figure 1b. In the present case the first stable bifurcated family is of multiplicity 5 and the secondary resonances are obtained from a Farey tree generated in the interval $[\frac{1}{1}, \frac{1}{2}]$ by multiplicating these rationals with $\frac{1}{5}$. In general the secondary bifurcations correspond to the rationals $\frac{1}{n}[\frac{1}{1}, \frac{1}{2}]$ where n is the multiplicity of family from which the other families bifurcate. Similarly from the secondary bifurcations third order bifurcations are born, and so on. All the resonances $\frac{1}{n}$ for $4 \leq n \leq 9$ behave in a similar way in the rotational map as the resonances $\frac{1}{4}$ and $\frac{1}{5}$. Thus they bifurcate from the central family for $\omega = \frac{1}{n}$ having n stable and n unstable fixed points and they undergo a sequence of period doubling bifurcations. A hierarchy of resonances of higher order multiplicities is can also be found.

The different behavior of the resonance $\frac{1}{3}$ can be completely understood by calculating the characteristic of this resonance. This characteristic has its minimum value at $\omega_{3\ \min} = 0.31797168$ (Figure 7a). This minimum (with respect to ω) is not on the central characteristic but at a finite distance from it (Figure 7b) and the stability index of the corresponding fixed point is equal to $+1$. This result for a 2-D hamiltonian system has been found by Contopoulos [20] analytically by means of a 'third' integral of motion. We remark that the tangent of the characteristic $\frac{1}{3}$ at $\omega_{3\ \min}$ is perpendicular to the central characteristic since this central family coincides with ω axis. The characteristic, as ω increases, consists of a stable and an unstable branch (Figure 7b). For $\omega = \omega_3$ the stable branch become unstable at a finite distance from the central family and the value of the stability index is -1. Thus we obtain a sequence of period doubling bifurcations which we follow for five successive bifurcations up to the family with multiplicity 192 (Figure 7a).

Following these successive bifurcations for greater multiplicities we found that for $\omega = \omega_{3\delta} = 0.33551152090681$ all the families of this sequence become unstable. The 'universal ratio' is found to be $\delta = 8.7209\ldots$. All the unstable families go to infinity, as $\omega \to \frac{1}{2}$. Also, as in the other resonances discussed above, secondary and higher order resonances of multiplicities $\frac{1}{3}[\frac{1}{1}, \frac{1}{2}]$ for ω ranging in the interval $[\omega_{3\ \min}, \omega_3]$ are generated from the stable branch of the bifurcating families. On the other hand the unstable branch, corresponding to hyperbolic fixed points going towards the central family intersects it obliquely at ω_3 (Figure 7b) and thus we understand the non existence of invariant curves around the stable fixed point of the central family, in agreement with the behavior observed from the corresponding phase portrait. As ω increases further beyond ω_3 the unstable branch remains unstable escaping to infinity.

Similar results for the characteristic curves of the type $\frac{m}{3}$ have been obtained explicitly by Contopoulos [20] for a 2-D hamiltonian system, using normal forms. The difference compared to our case is that the tangent of the characteristic $\frac{1}{3}$ at its minimum is not perpendicular to the central family, as it is in the quadratic map (Figure 7b). This is due to the fact that in the quadratic map the central family and the ω-axis coincide.

A consequence of the behavior of the resonance $\frac{1}{3}$ is that for values of ω smaller than ω_3 many resonances bifurcate inversely [13,20], i.e. the characteristics of families with $\frac{m}{n} < \frac{1}{3}$ (but close to $\frac{1}{3}$) open up (like the branches of a hyperbola) towards smaller values of ω instead of opening up towards larger values of ω as in all other cases. A first estimation of the values of ω at which such inverse bifurcations occur can be found in the quadratic map, because the tangent at the minimum of the characteristic is perpendicular to the central family, by constructing a Farey tree in the intervals $[\frac{69}{217}, \frac{7}{22}]$ and $[\frac{7}{22}, \frac{1}{3}]$ which corresponds to values of ω in the interval $[\omega_{3\ \min}, \omega_3]$. But investigating numerically, we found that all the bifurcating resonances corresponding to the rationals of the Farey tree for $\omega \in [\frac{4}{13}, \frac{1}{3}]$ are inverse. The limits are not exact but the resonance $\frac{4}{13}$ exists for $\omega = 0.30765$ which is slightly smaller than $\omega = \frac{4}{13} \simeq 0.30769$. Thus inverse bifurcations exist for values even smaller than $\omega_{3\ \min}$ while bifurcations for $\omega > \omega_3$ are direct.

An interesting result concerning the stability character of the resonances $\frac{1}{3}, \frac{1}{4}$ and $\frac{1}{5}$ is obtained. As we discussed, in all cases the corresponding families are initially (with respect to ω) stable and we found the values of ω at which they become unstable. But, as ω tends to its limiting value $\frac{1}{2}$ the stability index of each family tends to the definite values -19.73, -155 and -950 respectively despite the fact that the corresponding fixed points go to infinity (Figure 8). We also observe that as the multiplicity of a resonance is smaller the corresponding limiting stability value is smaller.

We also notice an interesting consequence as a result of the behavior of the characteristic of the $\frac{1}{3}$ resonance. For almost any value of ω an area around the central fixed points is occupied by invariant curves. The only exception is at the

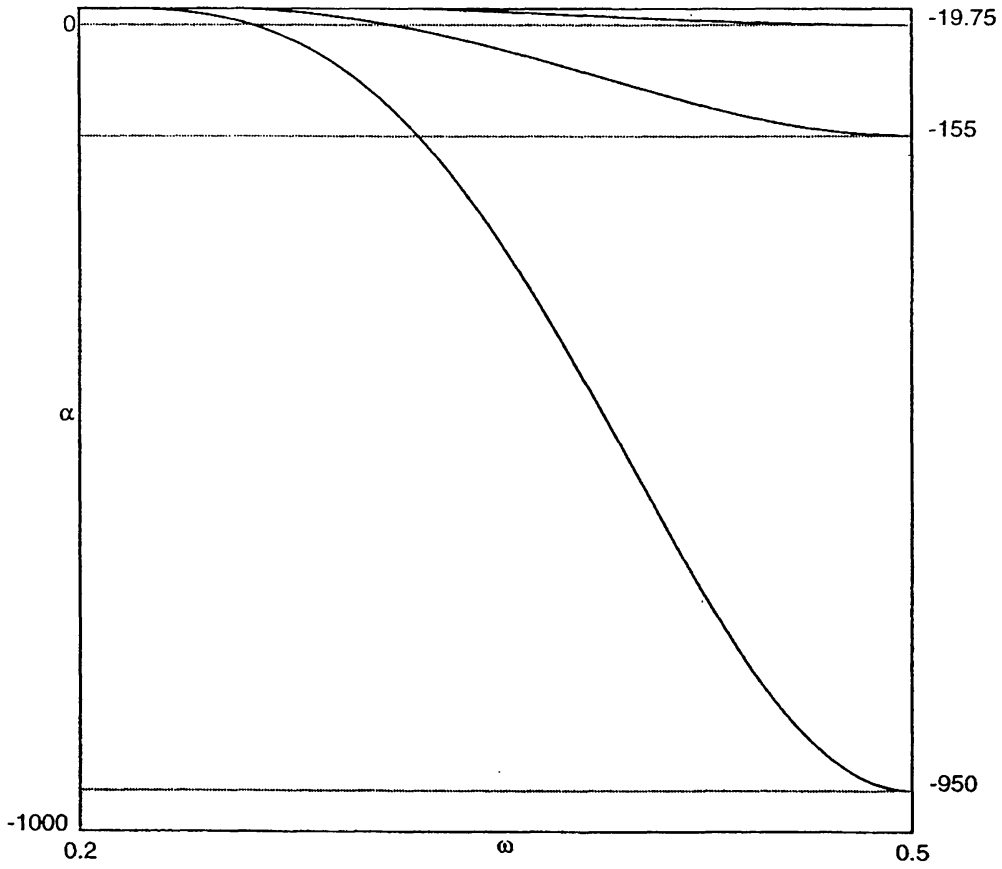

Figure 8. The Hénon stability indices of the resonances $\frac{1}{3}$, $\frac{1}{4}$ and $\frac{1}{5}$. In these cases the indices tend to a finite limit. The limits are -19.75, -155 and -950 respectively and we observe that they are different for different resonances.

value ω_3. At this value no invariant curves surrounding the central fixed point exist. That is, as $\omega \to \frac{1}{3}$ from smaller or greater values the area occupied by invariant curves decreases and tends to$\to$ 0. On the other hand inverse bifurcations occur only for values of ω smaller than ω_3 and it is known that such bifurcations are of physical interest because they largely influence the transport mechanisms and the diffusion properties of a dynamical system [14].

In the 'beam-beam' map we calculated the characteristics of some resonances. We notice that the behavior of the resonant characteristics of the 'beam-beam' map deserves a more detailed study that will be done in the future.

We found that all resonances, as ω increases, behave in a completely different way with respect to the rotational map. In the 'beam-beam' map the characteristics extend far from the origin, but they do not escape as they do in the quadratic map. This is due to the boundedness of $h(x)$ for large $|x|$. In general, the fixed points of any resonance, as ω increases, reach regions of the phase plane where $h(x)$ starts behaving in a significantly different fashion with respect to x^2. A difference, between the quadratic and the 'beam-beam' maps concerns the period doubling bifurcations. Our first calculations show us that the first bifurcating families from

several resonances, e.g the resonances $\frac{1}{3}$ and $\frac{1}{5}$, are not of double but of equal period.

We notice the behavior of the resonance $\frac{1}{3}$ in the 'beam-beam' map which is again peculiar as in the rotational one. It appears for $\omega'_{3\ \min} = 0.3203204 < \omega_3$ in a finite distance from the central family. The stable branch moves away from the central family but it does not become unstable for $\omega = \omega_3$ as it does in the quadratic map, while the unstable one moves towards the central family as in the quadratic map. Thus in the 'beam-beam' map inverse bifurcations exist too. By doing an analysis similar to the one for the quadratic map, we find that the inverse bifurcations correspond to a Farey tree for $\omega \in [\frac{7}{22}, \frac{1}{3}]$.

A significant result is obtained by comparing the inverse bifurcating resonances of both maps. The resonances $\frac{m}{n}$ which correspond to the rationals in the interval $[\frac{4}{13}, \frac{7}{22}]$ are inverse in the rotational map and direct in the 'beam-beam' map, although both maps have the same linear part.

5. Conclusions

The Hénon qudratic conservative map is a basic model with applications in many physical problems. Thus it is of considerable interest to understand the dynamical behaviour of this map.

We investigated in detail many families of fixed points of the rotational map (2) by calculating the corresponding characteristic curves. In particular we have calculated the characteristics of the resonant periodic orbits of the type $\frac{1}{n}$, for $3 \leq n \leq 9$.

We define a class of maps with same linear parts as the Hénon qudratic map. Thus the bifurcating families from the central family are the same for all these Hénon like maps. We made a first general discussion for one of them, the so called 'beam-beam' map.

The algorithm used for finding the positions of fixed points of high multiplicity and their stability character is very efficient and accurate. The method works very well, and it is suitable for quantitative investigation of any other class of conservative maps of the plane onto itself and for two degrees of freedom hamiltonian systems.

Our conclusions for the rotational map complete Hénon [1] and are complementary of Bountis [4] results. Thus in the following main conclusions for the quadratic map we consider also the behavior of the resonance of multiplicity 2 which is studied by Bountis but not by Hénon.

The Hénon stability index of the central family decreases monotonically from $+1$ to -1 as the parameter ω increases in its domain $[0, \frac{1}{2}]$, which means that the central family is stable. Thus an infinity of resonances $\frac{m}{n}$ where m, n are prime integers and $m < n$,$n \geq 1$, bifurcate from the central family. These resonances are of the second genus and they correspond to Poincaré's 'deuxième genre' families for hamiltonian systems. All the second genus resonances $\frac{m}{n}$ correspond to a Farey

tree with zeroth interval $[\frac{0}{1}, \frac{1}{2}]$. There also exist secondary and even higher order resonances. They are born from the stable parts of the bifurcating families and they correspond to Farey trees with zeroth generation $\frac{1}{n}[\frac{1}{1}, \frac{1}{2}]$ where n is the multiplicity of any higher order resonance.

The $\frac{1}{3}$ resonant characteristic bifurcates by crossing obliquely the central one. It is unstable on both sides of the intersection and its minimum, with respect to the parameter, is at finite distance from the central family. The minima of all other resonances are located on the central family. These results are valid for the 'beam-beam' map also. Thus in both maps the behavior of the $\frac{1}{3}$ resonance is peculiar. This peculiarity has also been found analytically in a 2-D hamiltonian system and seems to be general for 2-D dynamical systems.

Families bifurcating inversely are born from the central one for values of ω smaller than the value at which bifurcates the resonance $\frac{1}{3}$. This is true for both maps. Thus we conjecture that the region occupied by regular motion and the diffusion properties are differently influenced depending on whether the values of ω are smaller or greater than $\frac{1}{3}$.

We also found, as regards the inverse bifurcations, an important result. There exist resonances which bifurcate inversely in the quadratic map but the same resonances bifurcate directly in the 'beam-beam' one, although both maps possess the same linear part.

In the quadratic map all the bifurcated elliptic points become hyperbolic, at a finite distance from the origin. Then all fixed points as the parameter increases escape to infinity as unstable. The value of the parameter at which each stable family become unstable is different for each resonance and a sequence of period doubling bifurcations is produced. The ratio of the successive intervals of the parameter values at which the bifurcations occur tends to the well known 'universal value'.

The stability index of the principal bifurcations tends asymptotically to a finite value despite the fact that the corresponding fixed points escape to infinity. This value becomes smaller as the multiplicity of the resonance gets smaller.

Another important result for the quadratic map as it is adopted by Bountis [4] is obtained by combining some of the above conclusions. The central family becomes unstable when the parameter a of equation (3) becomes $a = 1$. The bifurcating family of multiplicity 2 exists for greater values of the parameter and this generates families of multiplicity $s \cdot 2^k$ (where s, k are positive integers). All these families exist only for $a > 1$. When they are unstable they cannot have heteroclinic intersections with the unstable families above, which are generated for $a < 1$. Thus transport phenomena and diffusion process on the phase plane can not happen between the resonances of multiplicities 2^k that exist for $a > 1$ and the resonances that exist for $a < 1$. However transport phenomena exist either among resonances of different multiplicities for the parameter values at which the central family is stable ($a < 1$) or among resonances with multiplicities 2^k which exist for parameter values at which the central family is unstable ($a > 1$).

The behavior of the characteristics in the 'beam-beam' map is the same with those of the rotational one, close to the origin, with the exception of an interval of parameter values at which the same resonances bifurcate directly in the 'beam-beam' map and inversely in the quadratic map. As the parameter of the system increases the characteristics behave in a completely different way from those of the quadratic map without escaping to infinity because this system is bounded. Consequently the behavior of the homoclinic and heteroclinic tangles in each map will be different and thus the transport mechanisms and the diffusion process will also be different.

We notice that in the quadratic map the behavior of the resonances $\frac{m}{n}$ with $m > 1$ and $n \geq 3$, the inverse bifurcations, the homoclinic tangles and the heteroclinic intersections as well as the transport phenomena are open problems. As regards the 'beam-beam' map, many problems are still open too. They are under study and we hope to report on them in the future.

Appendix

We consider the area preserving map (1) depending on the real parameter ω, with $h(x) = x^2$. Then the map (1) reads

$$\begin{aligned} x' &= x\cos(2\pi\omega) + (y + x^2)\sin(2\pi\omega) \\ y' &= -x\sin(2\pi\omega) + (y + x^2)\cos(2\pi\omega) \end{aligned} \tag{A1}$$

or, equivalently,

$$\begin{pmatrix} x \\ y \end{pmatrix}' = \mathbf{R}(\omega)\begin{pmatrix} x \\ y + x^2 \end{pmatrix}. \tag{A2}$$

In (A2) $\mathbf{R}(\omega)$ is the orthogonal matrix

$$\mathbf{R}(\omega) = \begin{pmatrix} \cos(2\pi\omega) & \sin(2\pi\omega) \\ -\sin(2\pi\omega) & \cos(2\pi\omega) \end{pmatrix}.$$

The Jacobian of the map (1) is given by the determinant of $\mathbf{R}(\omega)$ which is equal to one on the whole plane.

On the other hand we consider the polynomial map of the form

$$\begin{aligned} x' &= 1 - y + ax^2 \\ y' &= x. \end{aligned} \tag{A3}$$

The polynomial map (A3) is equivalent to the rotational map (A1) only when the parameter a ranges in the interval $(-3, 1)$ and $a \neq 0$. In such interval we can

identify our $\cos(2\pi\omega)$ with the value $1-\sqrt{1-a}$, while outside that interval the matrix $\mathbf{R}(\omega)$ can no longer be taken orthogonal.

The equivalence between the Hénon like maps in rotational (A1) and polynomial (A3) form is proven as follows: we consider first the two fixed points $\mathbf{x}_+$ and $\mathbf{x}_-$ of the map (A3) which read

$$\mathbf{x}_\pm \equiv \frac{1}{a}(1 \pm \sqrt{1-a}, 1 \pm \sqrt{1-a}), \tag{A4}$$

they are real only when $a \leq 1$ and, of course, $a \neq 0$. We call these fixed points central fixed points. Apply the translation of coordinates which brings the fixed point $\mathbf{x}_-$ in the origin; such point has the right limiting value $(\frac{1}{2}, \frac{1}{2})$ when $a \to 0$ and in the new coordinates, say (ξ, η), the map (A3), for any $a \leq 1$, reads

$$\begin{aligned} \xi' &= 2(1-\sqrt{1-a})\xi - \eta + a\xi^2 \\ \eta' &= \xi \end{aligned} \tag{A5}$$

or, equivalently,

$$\begin{pmatrix} \xi \\ \eta \end{pmatrix}' = \mathbf{S}\begin{pmatrix} \xi \\ \eta \end{pmatrix} + \begin{pmatrix} a\xi^2 \\ 0 \end{pmatrix} \tag{A6}$$

with

$$\mathbf{S} = \begin{pmatrix} 2(1-\sqrt{1-a}) & -1 \\ 1 & 0 \end{pmatrix} = \begin{pmatrix} 2\cos(2\pi\omega) & -1 \\ 1 & 0. \end{pmatrix} \tag{A7}$$

Requiring that the eigenvalues of $\mathbf{S}$ are complex conjugated of modules one we find:

$$\begin{aligned} \lambda_\pm &= 1-\sqrt{1-a} \pm i\sqrt{1-(1-\sqrt{1-a})^2} \\ &= \cos(2\pi\omega) \pm \sin(2\pi\omega) \quad -3 \leq a \leq 1. \end{aligned} \tag{A8}$$

Now it is possible to perform a new linear change of coordinates, calling

$$\begin{pmatrix} u \\ v \end{pmatrix} = \mathbf{U}^{-1}\begin{pmatrix} \xi \\ \eta \end{pmatrix} \tag{A9}$$

using the nonsingular matrices:

$$\mathbf{U} = \begin{pmatrix} -1 & 0 \\ -\cos(2\pi\omega) & \sin(2\pi\omega) \end{pmatrix} \tag{A10}$$

and consequently

$$\mathbf{U}^{-1} = -\frac{1}{\sin(2\pi\omega)}\begin{pmatrix}\sin(2\pi\omega) & 0\\ \cos(2\pi\omega) & -1\end{pmatrix}. \tag{A11}$$

Of cource $\sin(2\pi\omega) \neq 0$, which means that $a \neq -3$ and $a \neq 1$ as we can see from formula (A8)

We notice that

$$\mathbf{R}(\omega) = \mathbf{U}^{-1}\mathbf{S}U. \tag{A12}$$

Thus (A6) becomes:

$$\begin{pmatrix}u\\ v\end{pmatrix}' = \mathbf{R}(\omega)\begin{pmatrix}u\\ v\end{pmatrix} + \mathbf{R}(\omega)\mathbf{R}(-\omega)\mathbf{U}^{-1}\begin{pmatrix}a(\mathbf{U}_{11}u + \mathbf{U}_{12}v)^2\\ 0\end{pmatrix}$$

and finally

$$\begin{pmatrix}u\\ v\end{pmatrix}' = \mathbf{R}(\omega)\begin{pmatrix}u\\ v - \frac{1}{\sin(2\pi\omega)}u^2\end{pmatrix}. \tag{A13}$$

Then by putting

$$\begin{pmatrix}u\\ v\end{pmatrix} = -\frac{\sin(2\pi\omega)}{a}\begin{pmatrix}\hat{x}\\ \hat{y}\end{pmatrix} \tag{A14}$$

we get

$$\begin{pmatrix}\hat{x}\\ \hat{y}\end{pmatrix}' = \mathbf{R}(\omega)\begin{pmatrix}\hat{x}\\ \hat{y} + \hat{x}^2\end{pmatrix}$$

which is a map of the form (A2).

Thus the general transformation is:

$$\begin{pmatrix}x\\ y\end{pmatrix} = \frac{\cos(2\pi\omega)}{a}\begin{pmatrix}1\\ 1\end{pmatrix} - \frac{\sin(2\pi\omega)}{a}\begin{pmatrix}-1 & 0\\ -\cos(2\pi\omega) & \sin(2\pi\omega)\end{pmatrix}\begin{pmatrix}\hat{x}\\ \hat{y}\end{pmatrix} \tag{A15}$$

where $-3 < a < 1$ and $a \neq 0$. The parameters ω and a are related through

$$a = 1 - 4\sin^4(\pi\omega), \quad -3 < a < 1, \quad a \neq 0 \tag{A16}$$

On the other hand writing the map (A3) in the form

$$\begin{aligned} x' &= 1 - y - ax^2,\\ y' &= x, \end{aligned} \tag{A17}$$

we can transform it to (A1) following the same procedure, by putting $\cos(2\pi\omega) = 1 - \sqrt{1+a}$ with a ranging in the interval $(-1, 3)$ and $a \neq 0$. Then the relation between the parameters a and ω reads

$$a = -1 + 4\sin^4(\pi\omega), \quad -1 < a < 3, \quad a \neq 0. \tag{A18}$$

In this case the transformation is:

$$\begin{pmatrix} x \\ y \end{pmatrix} = -\frac{\cos(2\pi\omega)}{a}\begin{pmatrix} 1 \\ 1 \end{pmatrix} + \frac{\sin(2\pi\omega)}{a}\begin{pmatrix} -1 & 0 \\ -\cos(2\pi\omega) & \sin(2\pi\omega) \end{pmatrix}\begin{pmatrix} \hat{x} \\ \hat{y} \end{pmatrix}. \tag{A19}$$

Thus the study of the rotational map (A1) under the conditions (A16) or (A18) is equivalent to the study of the quadratic maps (A3) for $a \in (-3, 1)$ and $a \neq 0$, or (A17) for $a \in (-1, 3)$ and $a \neq 0$ respectively.

Acknowledgments

This work supported from the CEE grant Human Capital and Mobility N_r $ERBCHRXCT930330$. We wish to thank Professors G. Contopoulos and G. Turchetti for many useful discussions and for their comments and suggestions during the preparation of this work. One of the authors (Ch. S.) wishes to thank the Physics Department of Bologna University for the hospitality during this work.

References

1. Hénon, M.: 1969, *Quarterly of Appl. Math.* **XXVII**, 291.
2. Hénon, M.: 1976, *Comm. Math. Phys.* **50**, 69.
3. Bazzani, A., Servizi, G. and Todesco, E. and Turchetti, G.: 1994, *Normal Forms for Hamiltonian Maps and their Applications to Accelerator Physics*, CERN Yellow Reports **94-02**.
4. Bountis, T.: 1981, *Physica* **3D**, 577.
5. Contopoulos, G.: 1970, *Astron. J.* **75**, 96.
6. Contopoulos, G.: 1970, *Astron. J.* **75**, 108.
7. Benettin, G., Cercignani, C., Calgani, L. and Giorgilli, A.: 1980, *Lett. Al Nouvo Cim.* **28(1)**, 1.
8. Benettin, G., Calgani, L., Giorgilli, A.: 1980, *Lett. Al Nuovo Cim.* **29(6)**, 163.
9. Greene, J.M., MacKAY, R.S., Vivaldi, F. and Feigenbaum, M.J.: 1981, *Physica* **3D**, 468.
10. Bazzani, A., Bortolotti, D., Giovannozzi, M., Servizi, G., Todesco, E. and Turchetti, G.: 1995, *GIOTTO: an interactive program for the analysis of 2D area preserving maps* Fourth E.P.A.C. ed. by V. Suller et al. World Scientific 923.
11. Vrahatis, M.: 1988, *ACM Trans. Math.* Software **14**, 330.
12. Poincaré, H.: Nouvelle Méthodes de la Mécanique Céleste (Gauthier Villars, Paris, 1989) **Vol. 3**.
13. Contopoulos, G.: 1983, *Physica* **8D**, 142.
14. Polymilis, C. and Hizanidis, K.: 1993, *Phys. Rev. E* **47(6)**, 4381.
15. Contopoulos, G. and Polymilis, C.: 1993, *Phys. Rev. E* **47(3)**, 1546.
16. Hénon, M.: 1965, *Ann. d'Astroph.* **28(6)**, 992.
17. Moser, J.: 1958, *Astronom. J.* **63**, 439.
18. Siegel, C.L.: 'Vorlesungen uber Himmelsmechanik' (Springer-Verlag, Berlin, 1956), 203.
19. Feigenbaum, M.J.: 1980, '*Universal behavior in nonlinear systems*' Los Alamos Sci. **4**.
20. Contopoulos, G.: 1980, *Celest. Mech.* **22**, 403.